Side Chain and Backbone Dynamics of Phospholamban in Phospholipid Bilayers Utilizing ^{2}H and ^{15}N Solid-State NMR Spectroscopy†

Shadi Abu-Baker, Jun-Xia Lu, Shidong Chu, Clarke C. Brinn, Christopher A. Makaroff, and Gary A. Lorigan*

Department of Chemistry and Biochemistry, Miami University, Oxford, Ohio 45056.

Received April 20, 2007; Revised Manuscript Received July 30, 2007

ABSTRACT: ^{2}H and ^{15}N solid-state NMR spectroscopic techniques were used to investigate both the side chain and backbone dynamics of wild-type phospholamban (WT-PLB) and its phosphorylated form (P-PLB) incorporated into 1-palmitoyl-2-oleoyl-*sn*-glycerophosphocholine (POPC) phospholipid bilayers. ^{2}H NMR spectra of site-specific CD_3-labeled WT-PLB (at Leu51, Ala24, and Ala15) in POPC bilayers were similar under frozen conditions (−25 °C). However, significant differences in the line shapes of the ^{2}H NMR spectra were observed in the liquid crystalline phase at and above 0 °C. The ^{2}H NMR spectra indicate that Leu51, located toward the lower end of the transmembrane (TM) helix, shows restricted side chain motion, implying that it is embedded inside the POPC lipid bilayer. Additionally, the line shape of the ^{2}H NMR spectrum of CD_3-Ala24 reveals more side chain dynamics, indicating that this residue (located in the upper end of the TM helix) has additional backbone and internal side chain motions. ^{2}H NMR spectra of both WT-PLB and P-PLB with CD_3-Ala15 exhibit strong isotropic spectral line shapes. The dynamic isotropic nature of the ^{2}H peak can be attributed to side chain and backbone motions to residues located in an aqueous environment outside the membrane. Also, the spectra of ^{15}N-labeled amide WT-PLB at Leu51 and Leu42 residues showed only a single powder pattern component indicating that these two ^{15}N-labeled residues located in the TM helix are motionally restricted at 25 °C. Conversely, ^{15}N-labeled amide WT-PLB at Ala11 located in the cytoplasmic domain showed both powder and isotropic components at 25 °C. Upon phosphorylation, the mobile component contribution increases at Ala11. The ^{2}H and ^{15}N NMR data indicate significant backbone motion for the cytoplasmic domain of WT-PLB when compared to the transmembrane section.

Phospholamban (PLB)[1] is a 52-amino acid transmembrane protein that interacts with the Ca-ATPase pump and lowers its affinity for Ca^{2+} (*1*−*3*). PLB plays a major role in the regulation process of the cardiac cycle (contraction and relaxation), which controls the heartbeat (*3*−*5*). Unphosphorylated PLB inhibits sarcoplasmic reticulum ATPase activity and stops the flow of Ca^{2+} ions, and this inhibition can be relieved by the cyclic AMP- and calmodulin-dependent phosphorylation of PLB (*3*−*5*). Since PLB is biologically significant and it is relatively small, many theoretical and biophysical experimental studies have aimed to investigate its structure in a membrane (*6*−*22*).

On the basis of spectroscopic techniques and molecular modeling studies on pentameric WT-PLB, early structural reports on WT-PLB disagreed about whether the pentameric protein is composed of continuous α-helical subunits or composed of subunits that have two α-helices connected by an unstructured/β-sheet region (*8*, *21*). Recently, the Chou group revealed an unusual bellflower-like assembly for pentameric WT-PLB that indicates an α-helical cytoplasmic domain of the pentamer that on average points away from the membrane surface (Figure 1A) (*23*). Alternatively, recent results from the Middleton group suggest that the cytoplasmic domain of PLB (residues 1−23) is stabilized only through its association with the phospholipid bilayer surface (*24*). In addition, new solution and solid-state NMR spectroscopic studies on the AFA-PLB mutant monomer (where C36, C41, and C46 have been mutated to A36, F41, and A46, respectively) have been reported (*25*, *26*). The Veglia and Baldus groups debate whether the transmembrane domain of the monomeric AFA-PLB mutant structure is connected to an α-helical cytosolic segment that lies on and interacts with the membrane surface (L-shaped) (*25*) or a non-α-helical disordered cytosolic domain that has minimal interaction with the membrane surface (*26*).

Interestingly, the Veglia group resolved the solution NMR structure not only for the AFA-PLB monomer mutant (Figure 1B) but also for its phosphorylated form (*27*). The results of Veglia's new phosphorylation study indicate that phos-

† This work was supported by an AHA grant (0755602B) and a NIH Grant (GM080542). The 500 MHz wide bore NMR spectrometer was obtained from NSF Grant (10116333).

* To whom correspondence should be addressed. Phone: (513) 529-3338. Fax: (513) 529-5715. E-mail: garylorigan@muohio.edu.

[1] Abbreviations: P-PLB, phosphorylated phospholamban; PLB, phospholamban; TM-PLB, transmembrane domain of phospholamban; AFA-PLB, monomeric mutated form of PLB; SERCA, sarco(endo)-plasmic reticulum calcium ATPase; MLVs, multilamellar vesicles; POPC, 1-palmitoyl-2-oleoyl-*sn*-glycerophosphocholine; HCl, hydrochloric acid; TFE, 2,2,2-trifluoroethanol; NMR, nuclear magnetic resonance; CPMAS, cross-polarization magic-angle spinning; HPLC, high-performance liquid chromatography; MALDI-TOF, matrix-assisted laser desorption ionization time-of-flight mass spectrometry; SDS−PAGE, sodium dodecyl (lauryl) sulfate−polyacrylamide gel electrophoresis; IPTG, isopropyl β-D-1-thiogalactopyranoside; PMSF, phenylmethanesulfonyl flouride; MBP, maltose-binding protein.

10.1021/bi700749q CCC: $37.00 © 2007 American Chemical Society
Published on Web 10/02/2007

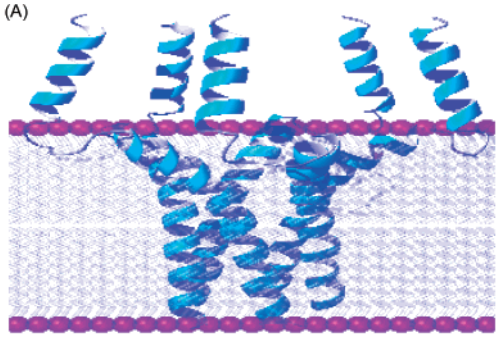

FIGURE 1: High-resolution solution NMR structures as well as the corresponding sequences for (A) pentameric (bellflower-like assembly) and (B) monomeric (L-shaped) phospholamban, by the Chou (*23*) and Veglia (*26*) groups, respectively. The two structures embedded inside membrane bilayers were generated using MOLMOL and a G5 Apple Mac computer. The three-dimensional structures in panels A and B were obtained from the Protein Data Bank.

phorylation of serine 16 (located within the cytoplasmic domain) induces an order-to-disorder transition that disrupts the "L-shaped" monomer and causes a reduction in the extent of α-helical secondary structure around the phosphorylation site (*27*). However, the Chou group has not determined the phosphorylated form (P-PLB) of WT-PLB (*23*). They proposed that introducing a negative charge upon phosphorylation of WT-PLB could alter the average orientation of the cytoplasmic domain and decrease its accessibility to the calcium pump (*23*). Also, this latest model of WT-PLB interacting with SERCA introduced by the Chou group suggests that tightness of the PLB pentamer (supercoiled Leu/Ile zipper) could allow its cytoplasmic domain to fit into and interact with the groove of the SERCA cytoplasmic domain without the energetic cost of removing a subunit from the pentamer (*23*). Conversely, an earlier model suggests that phosphorylation of WT-PLB at Ser16 or Thr17 reduces its level of electrostatic binding with the pump and favors the association of the PLB monomers interacting with SERCA into PLB pentamers that do not interact with the pump (*1*, *3*). Another recent model proposes that an allosteric interaction between the PLB monomer and SERCA takes place (*28*). Therefore, understanding the dynamic motion of WT-PLB with respect to the membrane is absolutely needed to completely describe the mechanism of binding of WT-PLB to Ca-ATPase. Complete knowledge of how different segments of phosphorylated and unphosphorylated PLB are moving within the membrane is essential for describing the mechanistic functions of the protein. EPR spectroscopic studies on the cytoplasmic domain of monomeric AFA-PLB have indicated large-scale dynamic changes (*29*). Also, Oxenoid and Chou hypothesized that this cytoplasmic domain motion is needed for WT-PLB/Ca-ATPase to function properly (*23*).

It is clear that the cytoplasmic segment secondary structure, orientation, dynamics, and interaction with the membrane and SERCA of WT-PLB and P-PLB are under serious debate. However, it is important to emphasize that the high-resolution NMR solution structures of the monomeric PLB mutant (AFA-PLB) and pentameric WT-PLB in micelles reported by the Veglia (*26*) and Chou (*23*) groups, respectively, represent two of the best and widely accepted membrane protein structures available in the literature (see Figure 1). In addition, although the effect of phosphorylation on the cytoplasmic domain of WT-PLB has not been completely addressed in the literature, the Chou group suggested that their structure of WT-PLB in micelles sets the stage for a series of future experiments aimed at characterizing the effect of phosphorylation on the orientation and dynamics of its cytoplasmic helix (*23*). Our previous study indicated that phosphorylation does not significantly change the α-helical secondary structure of WT-PLB, and this finding agrees with the results previously reported by Arkin and co-workers (*8*, *30*). In addition, that same report implies that P-PLB has less direct contact with the membranes than WT-PLB does (*30*).

To extend and complement previous studies and to reveal new information about the dynamic properties of WT-PLB and its phosphorylated form (P-PLB), we have conducted NMR studies with PLB. These new studies will provide important physiological and mechanistic information regarding the regulatory role of WT-PLB and it phosphorylated form in biological systems (*3*, *23*, *28*). This dynamic information is crucial for understanding its binding to Ca-ATPase and inhibition. In this article, ^{2}H and ^{15}N solid-state NMR spectroscopic studies are utilized to ascertain pertinent information about the backbone and side chain dynamics of WT-PLB in phospholipid bilayers. ^{2}H solid-state NMR spectroscopy is a powerful well-developed technique for studying the structural and dynamic properties of membrane proteins in phospholipid bilayers (*31*−*34*). The corresponding quadrupolar splitting and line shapes of the ^{2}H solid-state NMR spectra can be used to probe the molecular dynamics of the side chain of selectively labeled residues in site-specific ^{2}H-labeled integral membrane proteins (*35*−*40*). The primary amino acid sequence of full-length PLB has few alanines (mainly in the cytoplasmic domain, residues 1−15) and several leucines (the transmembrane domain, residues 23−52) along the length of the protein (*23*). In previous studies, methyl group motions have been well-characterized utilizing ^{2}H NMR studies of CD_3-labeled sites of alanines, valines, and leucines (*35*, *40*−*45*). For the isotopically labeled alanines (short aliphatic side chains), the deuterated methyl group (CD_3) rotates around the $C_\alpha-C_\beta$ bond (see Figure 2A) and allows the deuterons to make jumps between three sites described by a tetrahedral geometry (*46*). However, for Leu, the long aliphatic side chain can be isotopically labeled at the δ- and/or ε-CD_3 sites, and the deuterium NMR powder pattern line shapes will be strongly influenced by the motions about the $C_\gamma-C_\delta$ bond axis as well as by

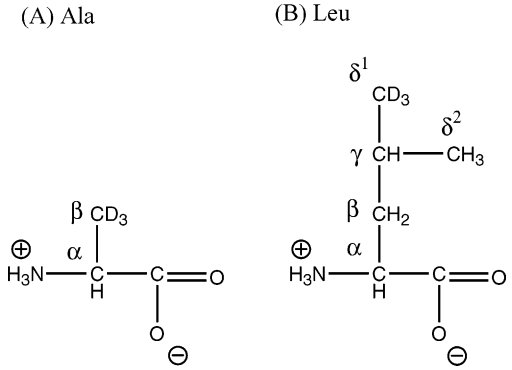

FIGURE 2: Chemical structure of the (A) alanine and (B) leucine amino acids.

additional librational motion about the $C_\alpha-C_\beta$ and $C_\beta-C_\gamma$ bond axes (see Figure 2B) at various temperatures (*40*, *47*). If the CD_3-methyl probe of the protein undergoes no motion other than those associated with the axial rotation about the $C-CD_3$ bond in a randomly dispersed sample, the resultant spectra will consist of a Pake pattern with a 40 kHz quadrupolar splitting (*48*). However, residues located outside the membrane are expected to be more motionally averaged and yield an isotropic peak (*49*).

Additionally, ^{15}N solid-state NMR spectroscopy has been used to ascertain direct information regarding backbone dynamics of membrane proteins (*45*, *50*). Generally, the immobile (without large amplitude motions) amide sites of specific ^{15}N-labeled proteins yield a broad static ^{15}N powder pattern, whereas motionally averaged amide sites reveal isotropic peaks (*50*).

MATERIALS AND METHODS

Materials. POPC was purchased from Avanti Polar Lipids (Alabaster, AL). Prior to use, phospholipids were dissolved in chloroform and stored at −20 °C. Chloroform, hexafluoro-2-propanol, formic acid, and 2,2,2-trifluoroethanol (TFE) were purchased from Aldrich Chemical Co. (St. Louis, MO). HPLC-grade acetonitrile and 2-propanol used to purify the protein were obtained from Pharmco (Brookfield, CT) and were filtered through a 0.2 μm nylon membrane before being used. Water was purified using a nanopure reverse osmosis system (Millipore, Bedford, MA). Fmoc amino acids, prephosphorylated Fmoc serine amino acid, and other chemicals for peptide synthesis were purchased from Novabiochem (San Diego, CA). ^{15}N- and CD_3-labeled Leu and Ala Fmoc amino acids, $^{15}NH_4Cl$, and deuterium-depleted water were purchased from Isotec/Sigma-Aldrich (St. Louis, MO). *N*-(2-Hydroxyethyl)piperazine-*N*′-2-ethanesulfonic acid (HEPES) and EDTA were obtained from Sigma-Aldrich.

Synthesis and Purification of Site-Specific CD_3- and ^{15}N-Labeled WT-PLB and P-PLB. WT-PLB was synthesized using a modified Fmoc-based solid-phase method with an ABI 433A peptide synthesizer (Applied Biosystems, Foster City, CA) as described in a previous report (*30*).

In this study, the isotopically labeled amino acids were chosen to cover both the cytoplasmic and transmembrane regions of WT-PLB embedded in the POPC MLVs. The CD_3-labeled sites were chosen (Leu51, Ala24, and Ala15), and the ^{15}N-labeled amide residues were chosen (Leu51, Leu42, and Ala11). To synthesize P-PLB, a prephosphorylated Fmoc serine amino acid was used at amino acid position 16 instead of the regular Fmoc serine used in the synthesis of WT-PLB (*51*). The crude peptide was purified on an Amersham Pharmacia Biotech AKTA explorer 10S HPLC system controlled by Unicorn (version 3) system software as described in a previous study (*30*). The purified protein was lyophilized and characterized by matrix-assisted laser desorption ionization time-of-flight (MALDI-TOF) mass spectrometry and SDS−PAGE (data not shown). In agreement with the work of Simmerman and co-workers (*52*), the oligomeric state of our PLB and P-PLB using SDS−PAGE was mainly pentameric and did not show the coexistence of any dimeric bands as reported for the AFA-PLB mutant (*12*).

Preparation of Uniformly ^{15}N-Labeled WT-PLB. The overexpression and purification of WT-PLB have been reported previously (*53*). In this study, a slightly modified procedure has been employed. In brief, the gene encoding wild-type PLB cloned into a modified pMalc2X vector was transformed into *Escherichia coli* BL21(DE3)-RIL (Stratagene). The starter culture was grown overnight in standard M9 minimal medium supplemented with vitamins (Sigma BME vitamin solution) and minerals [6 mg/L $FeSO_4$, 1.3 mg/L $MnSO_4$, 0.8 mg/L $CoCl_2$, 0.6 mg/L $ZnCl_2$, 0.3 mg/L $CuSO_4$, 0.02 mg/L H_3BO_3, 0.25 mg/L $(NH_4)_6Mo_7O_{24}$, and 5 mg/L EDTA]. Cells were then transferred (1:50) into fresh M9 minimal medium with $^{15}NH_4Cl$ as the sole nitrogen source. Cells were induced with 1 mM isopropyl β-D-1-thiogalactopyranoside (IPTG) when the absorption at 600 mn was approximately 0.7 ($OD_{600} \sim 0.7$). After growing overnight at 37 °C, cells were harvested and resuspended using 150 mL of lysis buffer [20 mM Tris-HCl (pH 8.0), 200 mM NaCl, 1 mM EDTA, 0.1 mM DTT, 0.5% glycerol, 2.5 mM lysozyme, and 0.5 mM phenylmethanesulfonyl flouride (PMSF)] per liter of culture. The suspension was passed twice through a French press and centrifuged at 38000*g* for 20 min at 4 °C. The supernatant containing the maltose-binding fusion protein MBP-PLB was purified using an amylose resin (New England Biolabs). PLB was released from MBP by cleavage using active tobacco etch virus protease (Ac-TEV) (Invitrogen) and subsequently purified by HPLC (Amersham Pharmacia Biotech) using a silica-based C4 reverse-phase column (Vydac). The purified protein was lyophilized and characterized by MALDI-TOF mass spectrometry and SDS−PAGE (see Figure 1S). Like the chemically synthesized site-specific isotopically labeled WT-PLB, the oligomeric state of uniformly ^{15}N-labeled WT-PLB determined using SDS−PAGE was predominantly pentameric.

NMR Sample Preparation. POPC bilayers containing 4 mol % P-PLB or WT-PLB in phospholipid were prepared according to the protocol given by Rigby and co-workers (*48*). POPC (35 mg) and PLB or P-PLB were dissolved in $CHCl_3$ and TFE, respectively, and placed into a 12 mm × 75 mm test tube. The solvents were removed under a steady stream of N_2 gas, and then the test tube was placed in a vacuum desiccator overnight to remove any residual solvent. The P-PLB/lipid or PLB/lipid mixture was then resuspended in 95 μL of HEPES buffer [5 mM EDTA, 20 mM NaCl, and 30 mM HEPES (pH 7.0)]. The buffer was prepared using deuterium-depleted water from Isotec/Sigma-Aldrich. Finally, after the phospholipids were fully dissolved, the sample was transferred to a 4 mm NMR rotor. The protein concentration that was used was 4 mol % for P-PLB or PLB with respect

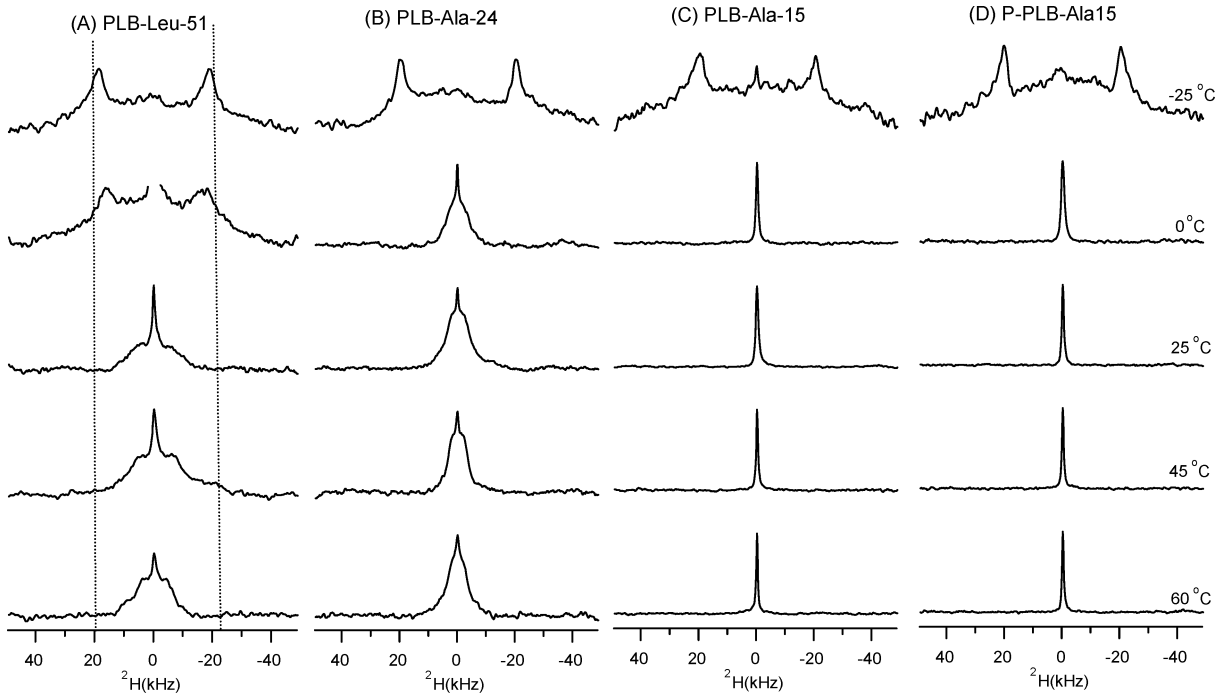

FIGURE 3: ^{2}H NMR powder pattern spectra of site-specific CD_3-labeled WT-PLB and its phosphorylated form embedded inside POPC phospholipid bilayers. ^{2}H NMR spectra are shown for (A) PLB-CD_3-Leu51, (B) PLB-CD_3-Ala24, (C) PLB-CD_3-Ala15, and (D) P-PLB-CD_3-Ala15. The experiments were conducted at temperatures ranging from −25 to 60 °C.

to lipids when both ^{15}N and ^{2}H NMR experiments were conducted.

Solid-State NMR Spectroscopy. A 500 MHz WB Bruker Avance solid-state NMR spectrometer and a Bruker 4 mm triple-resonance CP-MAS probe (Bruker, Billerica, MA) were used to collect the ^{2}H and ^{15}N solid-state NMR spectra. For ^{2}H solid-state NMR experiments, the spectrometer was operated at 76.77 MHz and the quadrupolar echo pulse sequence was employed using quadrature detection with complete phase cycling of the pulse pairs (*54*). The 90° pulse length was 3 μs, the interpulse delay 40 μs, the recycle delay 0.5 s, and the spectral width set to 100 kHz. To obtain a reasonable signal-to-noise ratio, a total of 25K (for the CD_3-Ala15 sample), 50K (for the CD_3-Ala24 sample), and 100K (for the CD_3-Leu51 sample) transients were averaged for each ^{2}H solid-state NMR spectrum. The spectra were processed using 100 Hz for the CD_3-Ala15 sample and 300 Hz line broadening for the other two spectra. To investigate the effect of residual deuterium in the buffer on the line shapes of the spectra, a control sample containing 4 mol % unlabeled WT-PLB was averaged for 25K, 50K, and 100K transients, and its spectra were compared to those of the CD_3-labeled PLB samples (see Figure 2S of the Supporting Information).

^{15}N solid-state NMR spectra were collected utilizing a RAMP cross-polarization pulse sequence with ^{1}H decoupling. The following pulse sequence parameters were used: 4.7 μs ^{1}H 90°, 1.5 ms contact time, 500 ppm sweep width, and a 4 s recycle delay. Also, 80K scans were averaged for the static ^{15}N CP experiments. The spectra were referenced to an external standard of $(^{15}NH_4)_2SO_4$ (27 ppm). The experiments were carried out at both 25 and −25 °C. Samples were spun at 5 kHz for the CP-MAS experiments.

Analysis of ^{2}H and ^{15}N Solid-State NMR Spectroscopic Data. To analyze the ^{2}H solid-state NMR data displayed in Figure 3, simulated spectra were generated by MXQET and are displayed in Figure 4 (*55*). The ^{2}H NMR spectral splitting ($\Delta\nu_Q$) described in eq 1 can be related to the motional characteristics of the site-specific CD_3 group-labeled peptide incorporated into randomly dispersed MLVs (*34*, *41*, *45*, *49*).

$$\Delta\nu_Q = \frac{3}{8}e^2Q\frac{q}{h}S_{mol}(3\cos^2\theta_i - 1) \quad (1)$$

where e^2Qq/h is the nuclear quadrupole coupling constant (165−170 kHz for a C−D bond) (*56*, *57*), S_{mol} is the molecular order parameter, describing orientational fluctuations of the C−D bond relative to the bilayer normal, and θ_i is the average orientation of each C−D bond relative to the bilayer normal (*34*, *41*, *45*, *49*).

For polycrystalline solids, all values of θ are possible and the quadrupolar splitting ($\Delta\nu$) is very large (for example, $\Delta\nu_Q$ is 127 kHz for CD_3-Leu solid aliphatic chains) (*38*, *58*). When the ^{2}H-labeled protein's backbone is completely immobile in MLVs, the corresponding ^{2}H power spectrum is expected to have a Pake doublet with a quadrupolar splitting of approximately 40 kHz indicating rapid rotation about the C−CD_3 bond. This splitting is expected at very low temperatures when all other types of motion are nearly frozen (*35*). The effect of CD_3-methyl group rotation along the C_α−C_β bond axis was studied using MXQET (see Figure 4A) (*55*). The simulations were generated by assuming that the deuterons of the CD_3-methyl group jump among 0°, 120°, and 240° around the C_α−C_β axes (*49*). Figure 4A shows that CD_3-methyl group hopping can reduce the quadrupolar splitting ($\Delta\nu$) from 121 kHz when the jump rate is 1×10^2 Hz to 45 kHz when the jump rate is in the range of $\geq 1 \times 10^7$ Hz.

The quadrupolar splitting value can be reduced further by different types of motions such as the "wobble" of the entire protein inside the MLVs, conformational fluctuations of the

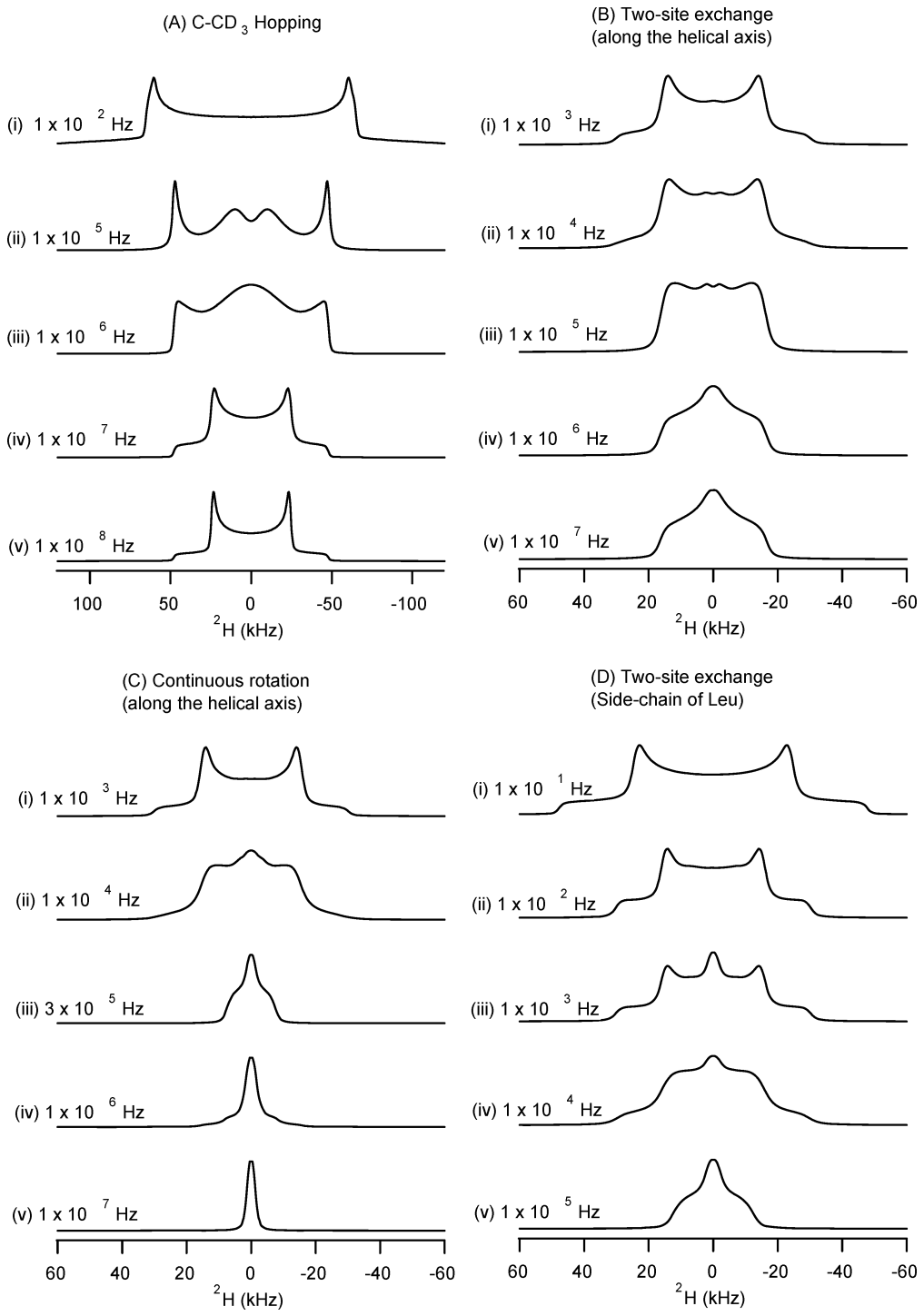

FIGURE 4: ^{2}H solid-state NMR spectral simulations using MXQET (*55*). In the generation of these spectra, rotations along the $C_\alpha-C_\beta$ bond axis (A), the long peptide helix axis (B and C), and the $C_\beta-C_\gamma$ bond axis (D) were considered, and the corresponding differences in ^{2}H NMR spectral line shapes and the quadrupolar splittings ($\Delta\nu$) were compared at different jumps rates. Panel A shows a 3-fold decrease in the quadrupolar splitting ($\Delta\nu$) when faster CD_3-methyl group hopping is considered. In panel A, only the CD_3-methyl group rotation about the $C_\alpha-C_\beta$ axis was considered. Panel B shows that faster two-site exchange along the peptide helix can gradually change the ^{2}H solid-state NMR spectral line shape from a typical Pake pattern to a bell-shaped pattern. In these simulations, the helix flips between two equally populated symmetry-related rotamers separated by 180°. This type of rotation does not affect the spectral splitting. (C) Simulation corresponding to continuous rotation along the long peptide helix which gradually changes the typical Pake pattern spectrum to an isotropic peak. In these simulations, the helix jumps among three equally populated symmetrical rotomers separated by 120°. Additionally, in panels B and C, the angle between the $C_\alpha-C_\beta$ bond of the CD_3-labeled alanine and the long helical axis of the was assumed to be 56°. (D) Simulation of the faster two-site methyl group jumping along the $C_\beta-C_\gamma$ bond axis of CD_3-Leu that generates a bell-shaped spectrum and decreases the quadrupolar splitting ($\Delta\nu$). In panel D, the methyl group was tilted by 75° and jumped by 109.5°.

protein backbone, rotation about the long axis of the peptide backbone, and other side chain internal motions (*35*, *59*). In panels B and C of Figure 4, only the anisotropic rotation about the protein long axis was considered for the simulations. Two modes of anisotropic rotation about the protein long axis at different rates were considered. In the first mode, the protein long helix axis flips between two equally populated symmetry-related rotamers separated by 180° (two-

site jump model), and in the second mode, it jumps among three equally populated symmetrical rotomers separated by 120° (continuous rotation model). For the CD_3-Ala residues, considering the rotation along the peptide backbone was enough to simulate the ^2H solid-state NMR spectra as indicated in a previous study (*12*). The angle between the $C_\alpha-C_\beta$ bond of CD_3-Ala and the long axis of the protein was assumed to be 56° (*12*). In Figure 4B, the two-site exchange along the long peptide helix can gradually change the typical Pake spectrum (jump rates in the range of 1×10^3 Hz) to a bell-shaped spectrum (generated using jump rates in the range of $\geq 1 \times 10^7$ Hz). Conversely, Figure 4C shows that continuous rotation along the long peptide helix can gradually change the typical Pake spectrum (jump rates in the range of 1×10^3 Hz) to an isotropic peak (jump rates in the range of $\geq 1 \times 10^7$ Hz).

Unlike Ala residues, the Leu side chain is longer. This allows the terminal CD_3 group of the Leu side chain to have two axes of librational rotation motion about the $C_\alpha-C_\beta$ and $C_\beta-C_\gamma$ bonds and a methyl group reorientation about the $C_\gamma-C_\delta$ bond (see Figure 2B). All of these dynamic motions affect the ^2H solid-state NMR spectra of ^2H-labeled proteins as described in the literature (*45*). In this study, we considered the tetrahedral methyl group hopping to be responsible for the first 3-fold decrease in the quadrupolar splitting (see Figure 4A). As a second axis of rotation, two-site methyl group jumping along the $C_\beta-C_\gamma$ bond axes in which methyl groups were tilted 75° and jumped by 109.5° was considered (see Figure 4D) (*45*). Figure 4D compares the line shapes of the generated ^2H solid-state NMR spectra at different two-site methyl group jump rates. The bell-shaped spectrum was generated at jump rates on the order of $\geq 1 \times 10^5$ Hz.

Simulations of the ^{15}N NMR spectra were carried out using DMFIT (*60*). The principle elements of the chemical shift tensors are represented according to the convention $\sigma_{33} \geq \sigma_{22} \geq \sigma_{11}$.

RESULTS

^2H Side Chain Dynamics. Figure 3 shows the solid-state ^2H NMR powder pattern spectra of site-specific CD_3-labeled WT-PLB (at residues Leu51, Ala24, and Ala15) and P-PLB (at residue Ala15) incorporated into POPC MLVs. The spectra were recorded over the temperature range from −25 to 60 °C. The corresponding simulated spectra generated by MXQET are displayed in Figure 4.

At −25 °C [below the lipid gel−liquid−crystalline phase transition temperature of POPC lipids (−3 °C)] (*61*), the four solid-state ^2H NMR powder pattern spectra reveal similar quadrupolar splittings ($\Delta\nu$) of ∼40 kHz, indicating that there is no significant difference in the dynamics of these residues at this low temperature. In the gel phase (−25 °C), the only significant motion is methyl group rotation, because global motion is not observed below the phase transition temperature of the lipid (*48*). Similar experimental ^2H line shapes and splitting have been reported in the literature at temperatures lower than the phase transition temperature of the lipids. Each spectrum can be simulated by considering only a CD_3-methyl group rotation along the $C-CD_3$ bond axis in the range of $\geq 1 \times 10^8$ Hz (see spectrum v in Figure 4A).

However, at 0 °C (slightly above the phase transition temperature), there are significant differences in the ^2H quadrupolar splittings as well as the line shapes among the four samples, indicating that the side chain motions of the PLB residues are different depending on the environment and position of these residues within the POPC membrane. In Figure 3A (at 0 °C), the Leu51 ^2H NMR spectrum reveals a quadrupolar splitting of ∼33 kHz and a line shape similar to that obtained for the same residue at −25 °C. The decrease in the ^2H quadrupolar splittings of the Leu51 spectrum at 0 °C can be attributed to rotational motion about the $C_\alpha-C_\beta$ and $C_\beta-C_\gamma$ axes. This spectrum can be simulated by considering an additional two-site methyl group jumping along the $C_\beta-C_\gamma$ bond axes in the range of 1×10^2 Hz when compared to the spectrum at −25 °C (see spectrum ii in Figure 4D). At higher temperatures (25, 45, and 60 °C), the ^2H quadrupolar splitting of the Leu51 spectrum (Figure 3A) is reduced along with significant spectral line shape changes when compared with those features of the spectrum at 0 °C, implying that additional librational motions about the $C_\alpha-C_\beta$ and $C_\beta-C_\gamma$ axes are occurring at higher temperatures. The spectra can be simulated by considering additional two-site methyl group jumping along the $C_\beta-C_\gamma$ bond axes of $>1 \times 10^5$ Hz (see spectrum v in Figure 4D).

In Figure 3B (at 0 °C), the ^2H NMR quadrupolar splitting (∼5 kHz) and line shape of Ala24 are completely different from those obtained for Leu51 at the same temperature. This ^2H NMR spectrum can be simulated using a continuous rotation model along the long peptide helix using jump rates in the range of 1×10^6 Hz (see spectrum iv in Figure 4C). The sharp isotropic peak from the residual deuterium in the buffer can affect the line shape of the experimental spectrum when compared to the simulated one (see Figure 2S of the Supporting Information). The significant differences in the line shape indicate that Ala24 and Leu51 are located in different environments. The large quadrupolar splitting of Leu51, which is located toward the lower end of the transmembrane helix, suggests that it is embedded inside the membrane. Previous studies have indicated that Leu51 is part of the pentameric WT-PLB zipper motif (*45*). All these factors restrict the side chain motion of this residue at 0 °C when compared to Ala24 which is located toward the upper end of the transmembrane helix.

Finally, the ^2H NMR spectra of ^2H-labeled Ala15 of both PLB (Figure 3C) and P-PLB (Figure 3D) at 0 °C exhibit isotropic spectral line shapes not typical of Pake doublets, due to additional motions associated with the location of this residue and/or backbone dynamics. These ^2H NMR spectra can be simulated using a continuous rotation model along the long peptide helix using jump rates of $>1 \times 10^7$ Hz (see spectrum v in Figure 4C). At higher temperatures (45 and 60 °C), the isotropic ^2H spectra (Figure 3C,D) are comparable with that at 25 °C.

^{15}N Backbone Dynamics. To investigate the backbone dynamics of PLB and P-PLB, site-specific ^{15}N-labeled proteins were incorporated into POPC MLVs and ^{15}N solid-state NMR spectroscopic experiments were conducted. The corresponding ^{15}N NMR spectra can distinguish between the rigid and mobile sites within the protein backbone on a time scale of 10^{-4} s (*50*). Large amplitude motions, which occur more rapidly than the breadth of the powder pattern spectra (^{15}N CSA breadth is $\sim 10^4$ Hz or 175 ppm), translate into a narrowing of the CSA width to an average isotropic position (*50*). To determine the degree of mobility of WT-PLB in

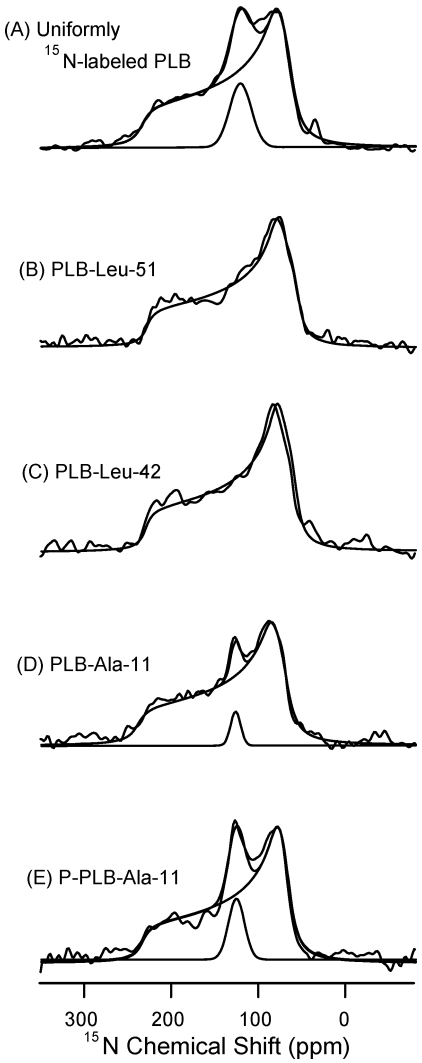

FIGURE 5: ^{15}N NMR powder pattern spectra of 4 mol % uniformly ^{15}N-labeled WT-PLB (A) as well as site-specific ^{15}N-labeled amide WT-PLB [Leu51 (B), Leu42 (C), and Ala11 (D)] and P-PLB [Ala11 (E)] proteins incorporated into POPC bilayers at 25 °C. The simulated spectra (A, D, and E) were generated by summation of its two components. The simulated spectra (B and C) were generated using one component.

Table 1: ^{15}N CSA Tensor Values of Uniformly ^{15}N-Labeled WT-PLB as Well as Site-Specifically ^{15}N-labeled WT-PLB (Leu51, Leu42, and Ala11) and P-PLB (Ala11) Inserted into POPC Phospholipid Bilayers at 25 °C

^{15}N site	σ_{11}	σ_{22}	σ_{33}	σ_{iso}	CSA width
uniformly labeled PLB	59.9	76.1	230.0	122.0	170.1
Leu51 of PLB	55.3	79.0	228.6	121.0	173.3
Leu42 of PLB	56.2	77.8	229.0	121.0	172.8
Ala11 of PLB	58.0	76.4	229.6	122.0	171.6
Ala11 of P-PLB	60.4	73.4	229.3	121.0	168.9

POPC bilayers at 25 °C, static ^{15}N cross-polarization experiments were conducted. Both the experimental (solid lines) and simulated spectra (dotted lines) are superimposed in Figure 5, and the chemical shift anisotropy (CSA) values extracted from those simulations are listed in Table 1 for comparison.

In Figure 5A, uniformly ^{15}N-labeled WT-PLB incorporated into POPC bilayers shows two distinct ^{15}N amide backbone components, a relatively narrow isotropic resonance and a broad well-defined powder pattern component. This indicates that WT-PLB has two different backbone dynamics components that can be observed on a time scale of 10^{-4} s (rigid and mobile sites). The contribution of the isotropic component of uniformly ^{15}N-labeled WT-PLB comes from two sources: the backbone dynamics of the cytoplasmic domain residues and the side chain dynamics of residues with long ^{15}N-labeled side chains such as arginine and lysine.

To distinguish between the different domains of WT-PLB, site-specific ^{15}N-labeled amide residues located on both the transmembrane (Leu51 and Leu42) and cytosolic (Ala11) domain of WT-PLB were incorporated into POPC bilayers and analyzed via solid-state NMR spectroscopy. Panels B and C of Figure 5 show that the site-specific ^{15}N-labeled amide residues located on the transmembrane domain (Leu51 and Leu42) yield only one broad powder pattern component, indicating that these sites are immobile on the NMR time scale in the POPC bilayers at 25 °C.

To investigate the effect of phosphorylation on the backbone mobility of the cytosolic domain of the protein, both WT-PLB and it phosphorylated form (P-PLB) were incorporated into POPC bilayers and static solid-state NMR spectra were collected. Figure 5D indicates that the ^{15}N-labeled Ala11 NMR spectrum of WT-PLB located on the cytoplasmic domain yields two dynamic components (powder pattern component and isotropic component), implying that the backbone dynamics of this residue exists in two populations: one that is immobile and another which is motionally averaged on the NMR time scale. Figure 5E shows that upon phosphorylation, the ^{15}N spectrum of ^{15}N-labeled Ala11 still consists of two populations; however, the population of the isotropic component has increased by a factor of 2 when compared to that of the unphosphorylated sample (Figure 5D).

To probe the effect of low temperature on the backbone mobility of the protein, uniformly ^{15}N-labeled WT-PLB as well as site-specific ^{15}N-labeled WT-PLB proteins were incorporated into POPC bilayers and the static ^{15}N NMR spectra were recorded at −25 °C. As expected, and in agreement with the ^{2}H data at −25 °C, all the samples revealed a static ^{15}N chemical shift powder pattern spectra indicating that the uniformly ^{15}N-labeled as well as the site-specific ^{5}N-labeled amide sites are all immobile at −25 °C. This confirms that the isotropic component observed for the cytoplasmic domain at 25 °C results from peptide backbone motion.

It has been reported that ^{15}N CP-MAS chemical shift values of ∼129 and ∼122 ppm (or less) are characteristic of β-sheet and α-helix structures, respectively (*62*). In this study, the values of the chemical shifts (at a spinning speed of 5 kHz) for the site-specific ^{15}N-labeled amide residues located on the cytosolic domain (Ala11) as well as the transmembrane domain (Leu51 and Leu42) were ≤122 ppm, implying that those residues located in both the transmembrane and cytosolic domains are relevant to α-helices of WT-PLB within POPC bilayers. Similar results were obtained for Ala11 of P-PLB, indicating that phosphorylation at Ser16 does not change the secondary structure of the cytoplasmic domain of WT-PLB around Ala11.

DISCUSSION

The focus of this study was to investigate the side chain and backbone dynamics of WT-PLB incorporated into POPC

bilayers as well as to probe any potential changes in dynamics of the cytoplasmic domain upon phosphorylation using ^{2}H and ^{15}N solid-state NMR spectroscopy. Previous conformational studies using a similar approach on an ion channel protein have been reported by Auger et al. (*63*). To better understand the data, we simulated both ^{2}H and ^{15}N experimental NMR spectra and extracted useful information about the jump rates as well as CSA values.

Side Chain Dynamics of CD_3-Labeled WT-PLB and P-PLB Incorporated into POPC Bilayers. The motions of the methyl groups in aliphatic side chains of selectively ^{2}H-labeled membrane proteins revealed pertinent side chain and backbone information (*38*−*40*, *44*, *47*, *58*, *59*, *64*). ^{2}H NMR line shapes of selectively ^{2}H-labeled proteins in membranes have been used to distinguish between residues buried inside the membrane and others located in the interface region (*31*). In addition, ^{2}H NMR spectral feature can be used to monitor the interactions between different transmembrane domains of membrane proteins and to investigate sites with restricted motions in the protein backbone (*41*, *48*, *65*). In a recent study by Hughes and co-workers, ^{2}H solid-state spectra of the monomeric AAA-PLB mutant (all the native cysteine residues were replaced with alanine residues) with CD_3-labeled Ala36 embedded inside the phospholipid bilayer were simulated (*12*). The investigators stated that the CD_3-methyl group rotation along the $C_\alpha-C_\beta$ axis is responsible for the 3-fold decrease in the quadrupole coupling constant from its typical value of ~170 kHz (*12*). As indicated in their study, rotation along the peptide backbone was enough to simulate the ^{2}H solid-state NMR spectra of CD_3-Ala in the transmembrane domain of the AAA-PLB monomeric mutant embedded inside the membrane (*12*). In their simulations, they considered two modes of anisotropic rotation about the protein long axis of the AAA-PLB protein (*12*). Similarly, in the simulations discussed in Figure 4B−D, a second axis of rotation was considered to describe the dynamic motions associated with the ^{2}H NMR spectrum. In general, the ^{2}H NMR line shape can be affected by several other factors other than those associated with the second axes of rotation along the long helical axis of the peptide (for CD_3-Ala) or $C_\beta-C_\gamma$ bond axes (for CD_3-Leu). Those other types of motions include (i) the wobble of the entire peptide in the membrane, (ii) finite conformational fluctuations of the peptide backbone, and (iii) side chain internal motions and librational averaging, including wobbling in a cone for the $C_\alpha-C_\beta$ bond (*48*, *66*). In addition, the depth of penetration of specific residues inside the membrane must be taken into consideration (*31*). Also, residues located outside the membrane are exposed to an aqueous environment (*31*).

The motions of the methyl group in the aliphatic side chain of Ala24 and Ala15 reveal pertinent side chain motions as well as backbone motions. This agrees with molecular dynamic simulations on PLB previously reported by Houndonougbe and co-workers (*10*). In that study, the researchers reported that the internal dynamics of the monomeric form of PLB is associated with large amplitude collective motions between the transmembrane and cytoplasmic helices (*10*). Those types of motions includes hinge bending, twisting of both N- and C-terminal helices, and flexing of the C-terminal helix (*10*). The central loop region is highly flexible and elastic (*10*). In their conclusion, they indicated that the twisting motions around the long helical axis enable PLB to adjust its structural topology and to orient the correct face of the helix to its binding site (*10*). In this study, the dramatic change in ^{2}H line shape between Ala15 and the residues (Leu51 and Ala24) buried in the membrane suggests that the cytoplasmic domain undergoes similar backbone motions as it is exposed to the aqueous environment outside the membrane and can be affected by twisting motions and other types of dynamics suggested by Houndonougbe and co-workers (*10*). In this study, no significant Ala15 side chain differences between WT-PLB and its phosphorylated form were detected in the ^{2}H solid-state NMR data analysis (Figure 3C,D). However, differences in the cytoplasmic backbone dynamics between WT-PLB and its phosphorylated form incorporated into POPC MLVs have been detected using ^{15}N solid-state NMR spectroscopy.

Backbone Dynamics of WT-PLB and Its Phosphorylated Form. The CSA tensor elements extracted from the ^{15}N simulations (see Figure 5) are listed in Table 1 for comparison. From the simulated spectrum (Figure 5A), the CSA width value of uniformly ^{15}N-labeled PLB was 170.1 ± 1 ppm. Also, for the site-specific ^{15}N-labeled amide WT-PLB at Leu51, Leu41, and Ala11 (Figure 5B−D), the CSA widths were 173.3 ± 1, 172.8 ± 1, and 171.6 ± 1 ppm, respectively. Additionally, the Leu51 and Leu41 spectra (Figure 5B,C) do not show any isotropic components. This indicates that Leu51 and Leu41 located in the transmembrane domain of WT-PLB are motionally restricted by interactions with the lipid membranes when compared to the Ala11 residue located in the cytoplasmic domain.

Moreover, Table 1 reveals that the CSA width value of ^{15}N-labeled Ala11 WT-PLB (Figure 5D,E) decreased from 171.6 ± 1 to 168.9 ± 1 ppm upon phosphorylation. Also, the integration of the two components (isotropic and powder) observed in the Ala11 spectra indicates that the contribution of the isotropic components of this labeled residue increases from 7 to 15% upon phosphorylation.

The isotropic peak of the [^{15}N]Ala11 spectrum suggests that the cytoplasmic domain exists in two conformations with different backbone dynamics on the ^{15}N solid-state NMR time scale; one conformation is mobile (outside the membrane), and another is rigid (most likely on the membrane surface). On the other hand, our ^{2}H Ala15 isotropic NMR data suggest that this residue is located outside the membrane. The dynamic isotropic nature of the peak can be attributed to side chain motions in an aqueous environment and backbone motion. It has been reported that residues located outside the membrane reveal isotropic ^{2}H NMR spectra (*31*). It is important to emphasize that ^{2}H solid-state NMR is more sensitive to different types of backbone and internal side chain motions associated with the protein on the ^{2}H solid-state NMR time scale, whereas ^{15}N solid-state NMR is sensitive to only the backbone motion of the protein on the ^{15}N NMR time scale. This observation was also reported for the Ala36 residue of the monomeric PLB mutant (*12*, *67*). Veglia and co-workers reported only a powder pattern ^{15}N solid-state NMR spectrum with no isotropic peaks for the ^{15}N-Ala36-PLB monomeric mutant (*67*). Conversely, Hughes and co-workers indicated using ^{2}H solid-state NMR that the monomeric form of the ^{2}H-Ala36-PLB mutant is associated with a ^{2}H NMR isotropic peak, implying that it rotates fast about its helical axis (*12*).

The motions of the methyl groups in aliphatic side chains reveal pertinent side chain and backbone motions. It has been reported previously that the epidermal growth factor receptor ($EGFR_{tm}$) monomer undergoes rapid axial diffusion about its long axes in the membrane (*48*). Dimerization or oligomerization likely gives rise to a subpopulation exhibiting slower axial rotation (*48*). Additionally, ^{2}H solid-state NMR provided a pertinent self-association (oligomerization) of the transmembrane domain of class I receptor tyrosine kinase (ErbB-2) in phospholipid bilayers (*34*). At high peptide concentrations, the CD_3-Ala spectral feature revealed multiple components that could be assigned to rapidly rotating transmembrane monomers (~8 kHz splitting), dimers (~24 kHz splitting), and large oligomers rotating very slowly relative to a time scale of 10^{-5} s (~38 kHz splitting) (*34*). Similarly, the ^{2}H NMR spectra of the transmembrane CD_3-Ala of the AAA-PLB mutant in lipid bilayers have been interpreted as representing a mixture of oligomeric and monomeric species (*12*). The bell-shaped component of the ^{2}H solid-state NMR spectra was considered to be the oligomeric species with slow rotation, and the other isotropic component was considered to be the monomeric species with fast rotation about the helical axis (*12*). In the study presented here, the ^{2}H solid-state NMR spectra of CD_3-Leu51 in the tramsmembrane region either have a typical Pake powder pattern at lower temperatures or are bell-shaped at higher temperatures, indicating that WT-PLB is pentameric and could rotate slowly about its helical axis. This implies that the significant ^{2}H spectral line shape changes of the Leu51 spectra (Figure 3A) at higher temperatures are related only to additional librational motions about the $C_\alpha-C_\beta$ and $C_\beta-C_\gamma$ axes. Although an isotropic component was observed, it can be attributed mainly to the residual deuterium in the buffer (see Figure 2S of the Supporting Information). However, it is possible that a slight contribution of this isotropic component may come from a minor monomoric component of the protein (see Figure 1S of the Supporting Information) rotating fast about its helical axis. Overall, the results indicate that the lower end of the transmembranes helix is predominantly immobile and embedded inside the membrane. This conclusion agrees with previous studies on the pentameric WT-PLB protein reported in the literature by the Smith group as will as the Lorigan group using ^{2}H solid-state NMR spectroscopy (*40*, *45*).

The effect of molecular motion along the long peptide axis of rotation on the ^{15}N powder pattern spectra has been described in detail elsewhere (*67*). Using computer simulations, the ^{15}N CSA widths and line shapes can change significantly with the rotation about the long helical axis of the protein (*67*). Recently, Hong and co-workers probed the effect of fast rotational diffusion of membrane peptides on the ^{15}N CSA width of powder samples. At 30 °C, the static ^{15}N solid-state NMR spectrum of a ^{15}N-labeled peptide incorporated inside DLPC bilayers revealed a ^{15}N CSA width of 105 ppm, indicating that the peptide undergoes fast uniaxial rotation (*68*). At −30 °C, the peptide returned to the rigid-limit ^{15}N CSA width of approximately 175 ppm (*68*). Conversely, the ^{15}N CSA for the transmembrane region of PLB decreased slightly at 25 °C when compared to that at −25 °C (see Figure 2S of the Supporting Information); therefore, our data are consistent with slow rotational diffusion of pentameric WT-PLB. SDS−PAGE gels clearly indicate that WT-PLB is more than 95% pentameric (see Figure 1S of the Supporting Information). On the basis of the ^{15}N data, we cannot completely rule out the presence of multiple oligomers (monomer and pentamer) of PLB. However, if we had a mixture of monomeric and pentameric species in our samples, we might expect to see two distinct components (with different ^{15}N CSA widths) on the static [^{15}N]Leu51 spectrum at room temperature. Because Leu51 is immobile in the pentameric species and part of the Leu/Ile zipper, the monomer species is expected to have a smaller ^{15}N CSA width. However, we do not see two different components in the ^{15}N CPMAS spectrum for Leu51 (see the Supporting Information). The data favor the existences of different conformations of WT-PLB. Nevertheless, it is still possible that a small amount of monomeric PLB may be contained within the samples.

The Cytoplasmic Domain of WT-PLB Exists in Two Structural Conformations with Distinct Dynamics. The ^{15}N and ^{2}H NMR data of the cytoplasmic domain alone (two conformers) do not completely rule out the presence of a monomer and pentamer in our PLB samples. Thses new ^{15}N data agree well with a recent study by the Lorigan group, where a ^{13}C═O site-specific (Ala15 residue) isotopically labeled WT-PLB protein inserted into POPC MLVs indicates that the PLB pentamer has two different α-helical structural conformations (*30*). Also, the Thomas group utilized EPR spectroscopy to probe AFA-PLB structural dynamics in lipid bilayers with the TOAC spin-label rigidly coupled to the peptide backbone (*29*). The corresponding EPR spectra measure the nanosecond peptide backbone dynamics in distinct domains of PLB (*29*). As expected for a well-ordered α-helix, their data indicate that residue 46 (located in the cytoplasmic domain of AFA-PLB) has a highly restricted rotational motion and a single well-defined ordered component (*29*). This agrees with the single ^{15}N powder component of Leu51 and Leu42 located in the transmembrane domain of the WT-PLB observed in this study. Furthermore, the most striking feature of their finding was the observation of two well-resolved conformational states (both α-helical ordered and partially unfolded disordered states) in the cytoplasmic domain at position 0 (~46% disordered) or 11 (only ~10% disordered) (*29*). The current ^{15}N solid-state NMR data agree with the two structural components of the WT-PLB pentamer observed by the Lorigan group (*30*) as well as with the Thomas group's two-conformation model on monomeric AFA-PLB (*29*). Furthermore, the new data suggest that upon phosphorylation, the disordered component doubles when compared to the unphosphorylated form of WT-PLB.

In another report, the Veglia group used ^{1}H−^{15}N heteronuclear solution NMR spectroscopic studies to probe the backbone dynamics of the AFA-PLB monomer (*19*). In that study, they did not directly resolve these two conformational states; however, the NMR spectroscopic data show evidence of an exchange process in the cytoplasmic domain of PLB in the micro- to millisecond time range that is consistent with the EPR spectroscopic studies (*19*).

Structural and Functional Implications of This Study on WT-PLB. The side chain dynamics of the transmembrane domain of the WT-PLB pentamer indicate that the upper part of the transmembrane domain is more dynamic that the lower part of the domain inside POPC bilayers (*19*). This observation agrees with a recent solution NMR report on the AFA-

PLB mutant. In that report, the investigators noted that residues 23−30 of the AFA-PLB monomer have significant flexibility when compared with the rest of the transmembrane (residues 31−52) segment (*19*). They propose that the plasticity of the upper part of the transmembrane domain of the AFA-PLB monomeric mutant could be a key factor that allows a relatively small membrane protein like PLB to adapt its conformation to several different targets by facilitating its recognition by several different proteins, including Ca-ATPase, protein kinase A, Ca/calmodulin-dependent kinase, and protein phosphatase (*19*). This elasticity and its significance could be also applied to the WT-PLB pentamer as well, especially in light of the latest model of WT-PLB interacting with SERCA (*23*). In that model, the Chou group proposes that the pentamer itself could interact with the groove of the SERCA cytoplasmic domain (see the introductory section for details) (*23*).

Additionally, the Thomas group proposes that the two-state dynamic equilibrium observed in their studies on the AFA-PLB monomeric mutant (between two conformations, ordered and disordered) is crucial for the function of the protein (*29*). Also, AFA-PLB function can be regulated by phosphorylation and by the protein's interaction with both SERCA and protein kinases (PKA) (*29*). Similarly, our backbone dynamic NMR data indicate that the two structural conformational models could be applied to the WT-PLB pentamer and that the functional WT-PLB pentamer could be regulated by phosphorylation as well.

CONCLUSION

In this study, several samples of site-specific isotopically labeled WT-PLB protein (CD_3-Leu51, CD_3-Ala24, CD_3-Ala15, ^{15}N-Leu51, ^{15}N-Ala42, and ^{15}N-Ala11) and its phosphorylated form, P-PLB (CD_3-Ala15 and ^{15}N-Ala11), as well as uniformly ^{15}N-labeled WT-PLB were successfully prepared and incorporated into POPC MLVs and studied with solid-state NMR spectroscopy. The ^{2}H NMR data indicate that the lower end of the TM helix shows restricted side chain motions when compared to the upper end of the helix. Moreover, additional motions were observed in the cytoplasmic helix when compared to the transmembrane domain. The isotropic peak indicates that the cytoplasmic domain undergoes large backbone motions. Also, the new ^{15}N NMR spectroscopic data indicate that the cytoplasmic domain consists of two different dynamic components (rigid and mobile components) when compared to the TM helix (which is immobile on the NMR time scale). Previously, the Chou group hypothesized that upon phosphorylation the introduced negative charge of the phosphate group at Ser16 could potentially alter the average orientation of the cytoplasmic domain of WT-PLB, leaving the helix less accessible to the calcium pump (*23*). Also, experiments by the Lorigan lab suggest a change in the orientation of the cytoplasmic domain of WT-PLB upon phosphorylation at Ser16 (*30*). In this study, a new observation indicates that phosphorylation increases the mobile component contribution and decreases the ^{15}N CSA value of the rigid component in the ^{15}N NMR spectrum when compared to the unphosphorylated form of WT-PLB. These findings agree with previous EPR (*29*) and solution NMR (*19*) studies on the AFA-PLB mutant, suggesting that the WT-PLB pentamer could function and be regulated in a manner similar to that of the AFA-PLB monomeric mutant.

ACKNOWLEDGMENT

We thank the Veglia and Thomas labs at the University of Minnesota (Minneapolis, MN) for the help with the preparation of uniformly ^{15}N-labeled WT-PLB.

SUPPORTING INFORMATION AVAILABLE

^{2}H NMR powder pattern spectra of four protein/POPC bilayers (Figure 1S) and ^{15}N NMR powder pattern spectra of 4 mol % uniformly ^{15}N-labeled WT-PLB and site-specific ^{15}N-labeled WT-PLB (Figure 2S). This material is available free of charge via the Internet at http://pubs.acs.org.

REFERENCES

1. Simmerman, H. K., Collins, J. H., Theibert, J. L., Wegener, A. D., and Jones, L. R. (1986) Sequence analysis of phospholamban: Identification of phosphorylation sites and two major structural domains, *J. Biol. Chem. 261*, 13333−13341.
2. Simmerman, H. K. B., Kobayashi, Y. M., Autry, J. M., and Jones, L. R. (1996) A leucine zipper stabilizes the pentameric membrane domain of phospholamban and forms a coiled-coil pore structure, *J. Biol. Chem. 271*, 5941−5946.
3. Simmerman, H. K. B., and Jones, L. R. (1998) Phospholamban: Protein structure, mechanism of action, and role in cardiac function, *Physiol. Rev. 78*, 921−947.
4. James, P., Inui, M., Tada, M., Chiesi, M., and Carafoli, E. (1989) Nature and site of phospholamban regulation of the calcium pump of sarcoplasmic reticulum, *Nature 342*, 90−92.
5. Kirchberger, M. A., Tada, M., and Katz, A. M. (1975) Phospholamban a regulatory protein of the cardiac sarcoplasmic reticulum, *Recent Adv. Stud. Card. Struct. Metab. 5*, 103−115.
6. Adams, P. D., Arkin, I. T., Engelman, D. M., and Brunger, A. T. (1995) Computational searching and mutagenesis suggest a structure for the pentameric transmembrane domain of phospholamban, *Nat. Struct. Biol. 2*, 154−162.
7. Arkin, I. T., Adams, P. D., Brunger, A. T., Smith, S. O., and Engelman, D. M. (1997) Structural perspectives of phospholamban, a helical transmembrane pentamer, *Annu. Rev. Biophys. Biomol. Struct. 26*, 157−179.
8. Arkin, I. T., Rothman, M., Ludlam, C. F. C., Aimoto, S., Engelman, D. M., Rothschild, K. J., and Smith, S. O. (1995) Structural model of the phospholamban ion-channel complex in phospholipid-membranes, *J. Mol. Biol. 248*, 824−834.
9. Fuji, J., Ueno, A., Kitano, K., Tanaka, S., Kadoma, M., and Tada, M. (1987) Characterization of structural unit of phospholamban by amino acid sequencing and electropherotic analysis, *Biochem. Biophys. Res. Commun. 138*, 1044−1050.
10. Houndonougbo, Y., Kuczera, K., and Jas, G. S. (2005) Structure and dynamics of phospholamban in solution and in membrane bilayer: Computer simulations, *Biochemistry 44*, 1780−1792.
11. Hubbard, J. A., Maclachlan, L. K., Meenan, E., Salter, C. J., Reid, D. G., Lahouratate, P., Humphries, J., Stevens, N., Bell, D., Neville, W. A., Murray, K. J., and Darker, J. G. (1994) Conformation of the cytoplasmic domain of phospholamban by NMR and CD, *Mol. Membr. Biol. 11*, 263−269.
12. Hughes, E., Clayton, J. C., and Middleton, D. A. (2005) Probing the oligomeric state of phospholamban variants in phospholipid bilayers from solid-state NMR measurements of rotational diffusion rates, *Biochemistry 44*, 4055−4066.
13. Hughes, E., and Middleton, D. A. (2003) Solid-state NMR reveals structural changes in phospholamban accompanying the functional regulation of Ca^{2+}-ATPase, *J. Biol. Chem. 278*, 20835−20842.
14. Kovacs, R. J., Nelson, M. T., Simmerman, H. B. K., and Jones, L. R. (1988) Phospholamban forms calcium selective channels in lipid bilayers, *J. Biol. Chem. 263*, 18364−18368.
15. Lamberth, S., Schmid, H., Muenchbach, M., Vorherr, T., Krebs, J., Carafoli, E., and Griesinger, C. (2000) NMR solution structure of phospholamban, *Helv. Chim. Acta 83*, 2141−2152.
16. Li, H. M., Cocco, M. J., Steitz, T. A., and Engelman, D. M. (2001) Conversion of phospholamban into a soluble pentameric helical bundle, *Biochemistry 40*, 6636−6645.

17. Li, J. H., Xiong, Y. J., Bigelow, D. J., and Squier, T. C. (2004) Phospholamban binds in a compact and ordered conformation to the Ca-ATPase, *Biochemistry 43*, 455−463.
18. Lockwood, N. A., Tu, R. S., Zhang, Z. W., Tirrell, M. V., Thomas, D. D., and Karim, C. B. (2003) Structure and function of integral membrane protein domains resolved by peptide-amphiphiles: Application to phospholamban, *Biopolymers 69*, 283−292.
19. Metcalfe, E. E., Zamoon, J., Thomas, D. D., and Veglia, G. (2004) H-1/N-15 heteronuclear NMR spectroscopy shows four dynamic domains for phospholamban reconstituted in dodecylphosphocholine micelles, *Biophys. J. 87*, 1205−1214.
20. Mueller, B., Hunter, G. W., Karim, C. B., and Thomas, D. D. (2003) FRET detection of Ca-ATPase and phospholamban interaction in membranes, *Biophys. J. 84*, 264A.
21. Tatulian, S. A., Jones, L. R., Reddy, L. G., Stokes, D. L., and Tamm, L. K. (1995) Secondary structure and orientation of phospholamban reconstituted in supported bilayers from polarized attenuated total-reflection FTIR spectroscopy, *Biochemistry 34*, 4448−4456.
22. Zhang, X. M., Kimura, Y., and Inui, M. (2004) Effects of phospholipids on the oligomeric structure of phospholamban (PLN), a regulator of Ca^{2+}-ATPase of cardiac sarcoplasmic reticulum (SR), *J. Pharm. Sci. 94*, 109P−109P.
23. Oxenoid, K., and Chou, J. J. (2005) The structure of phospholamban pentamer reveals a channel-like architecture in membrane, *Proc. Natl. Acad. Sci. U.S.A. 102*, 10870−10875.
24. Clayton, J. C., Hughes, E., and Middleton, D. A. (2005) The cytoplasmic domains of phospholamban and phospholemman associate with phospholipid membrane surfaces, *Biochemistry 44*, 17016−17026.
25. Andronesi, C. A., Becker, S., Seidel, K., Heise, H., Young, H. S., and Baldus, M. (2005) Detemination of membrane protein structure and dynamics by magic-angle-spinning solid-state NMR spectroscopy, *J. Am. Chem. Soc. 127*, 12965−12974.
26. Zamoon, J., Mascioni, A., Thomas, D. D., and Veglia, G. (2003) NMR solution structure and topological orientation of monomeric phospholamban in dodecylphosphocholine micelles, *Biophys. J. 85*, 2589−2598.
27. Metcalfe, E. E., Traaseth, N. J., and Veglia, G. (2005) Serine 16 phosphorylation induces an order-to-disorder transition in the monomeric phospholamban, *Biochemistry 44*, 4386−4396.
28. Zamoon, J., Nitu, F., Karim, C., Thomas, D. D., and Veglia, G. (2005) Mapping the interaction surface of a membrane protein: Unveiling the conformational switch of phospholamban in calcium pump regulation. *Proc. Natl. Acad. Sci. U.S.A. 102*, 4747−4752.
29. Karim, C. B., Kirby, T. L., Zhang, Z. W., Nesmelov, Y., and Thomas, D. D. (2004) Phospholamban structural dynamics in lipid bilayers probed by a spin label rigidly coupled to the peptide backbone, *Proc. Natl. Acad. Sci. U.S.A. 101*, 14437−14442.
30. Abu-Baker, S., and Lorigan, G. A. (2006) Phospholamban and its phosphorylated form interact differently with lipid bilayers: A ^{31}P, ^{2}H, and ^{13}C solid-state NMR spectroscopic study, *Biochemistry 45*, 13312−13322.
31. Koenig, B. W., Ferritti, J. A., and Gawrisch, K. (1999) Site-specific deuterium order parameters and membrane-bound behavior of a peptide fragment from the intracellular domain of HIV-1 gp-41, *Biochemistry 38*, 6327−6334.
32. Mack, J. W., Torchia, D. A., and Steinert, P. M. (1988) Solid-state NMR studies of the dynamics and structure of mouse keratin intermediate filaments, *Biochemistry 27*, 5418−5426.
33. Prosser, R. S., Daleman, S. I., and Davis, J. H. (1994) The structure of an integral membrane peptide: A deuterium NMR-study of gramicidin, *Biophys. J. 66*, 1415−1428.
34. Sharpe, S., Barber, K. R., Grant, C. W. M., and Morrow, M. R. (2002) Evidence of a tendancy of self-association of the transmembrane domain of ErbB-2 in fluid phospholipid bilayers, *Biochemistry 41*, 2341−2352.
35. Batchelder, L. S., Sullivan, C. E., Jelinski, L. W., and Trochia, D. A. (1982) Characterization of leucine side-chain reorientation in collagen-fibrils by solid-state deuterium NMR, *Proc. Natl. Acad. Sci. U.S.A. 79*, 386−389.
36. Beshah, K., Olejniczak, E. T., and Griffin, R. G. (1987) Deuterium NMR study of methyl dynamics in L-alanine, *J. Chem. Phys. 86*, 4730−4736.
37. Keniry, M. A., Kintanar, A., Smith, R. L., Gutowsky, H. S., and Oldfield, E. (1984) Nuclear magnetic resonance relaxation of deuteriomethyl-labeled amino acids crystals and in *Halobacterium halobium* and *E. coli* cell membranes, *Biochemistry 23*, 288−298.
38. Kinsey, R. A., Kintanar, A., and Oldfield, E. (1981) Dynamics of amino acid side-chains in membrane proteins by high field solid-state deuterium nuclear magnetic resonance spectroscopy, *J. Biol. Chem. 256*, 9028−9036.
39. Leo, G. C., Colnago, L. A., Valentine, K. G., and Opella, S. J. (1987) Dynamics of fd coat protein in lipid bilayers, *Biochemistry 26*, 854−862.
40. Ying, W., Irvine, S. E., Beekman, R. A., Siminovitch, D. J., and Smith, S. O. (2000) Deuterium NMR reveals helix packing interactions in phospholamban, *J. Am. Chem. Soc. 122*, 11125−11128.
41. Jones, D. H., Rigby, A. C., Barber, K. R., and Grant, W. M. (1997) Oligomerization of EGF receptor transmembrane domain: A ^{2}H NMR study in lipid bilayers, *Biochemistry 36*, 12616−12624.
42. Killian, J. A., Taylor, M. J., and Koeppe, R. E. (1992) Orientation of valine-1 side-chain of the gramicidin transmembrane channel and implications for channel functioning: A deuterium NMR study, *Biochemistry 31*, 11283−11290.
43. Lee, K. C., Huo, S., and Cross, T. A. (1995) Lipid-peptide interface: Valine conformation and dynamics in gramicidin channel in a lipid bilayer, *Biochemistry 34*, 857−867.
44. Van der Wel, P. C. A., Strandberg, E., Killian, J. A., and Koeppe, R. E. (2002) Geometry and intrinsic tilt of a tryptophan-anchored transmembrane α-helix determined by H-2 NMR, *Biophys. J. 83*, 1479−1488.
45. Tiburu, E. K., Dave, P. C., Damodaran, K., and Lorigan, G. A. (2004) Investigating Leucine Side-Chain Dynamics and Backbone Conformations of Phospholamban Incorporated in Phospholipid Bilayers Utilizing ^{2}H and ^{15}N Solid-State NMR Spectroscopy, *Biochemistry 43*, 13899−13909.
46. Batchelder, L. S., Niu, C. H., and Torchia, D. A. (1983) Methyl reorientation in polycrystaline amino acids in peptides, *J. Am. Chem. Soc. 105*, 2228−2231.
47. Janin, J., and Wodak, S. (1978) Conformation of amino acid side-chain in proteins, *J. Mol. Biol. 125*, 357−386.
48. Rigby, A. C., Barber, K. R., Shaw, G. S., and Grant, C. W. M. (1996) Transmembrane region of the epidermal growth factor receptor: Behavior and interactions via ^{2}H NMR, *Biochemistry 35*, 12591−12601.
49. Gibbons, W. J., Krap, E. S., Cellar, N. A., Minto, R. E., and Lorigan, G. A., Jr. (2006) Solid-state NMR studies of a diverged microsomal amino-proximate Δ12 desaturase peptide reveal causes of stability in bilayer: Tyrosine anchoring and arginine snorkeling, *Biophys. J. 90*, 1249−1259.
50. Colnago, L. A., Valentine, K. G., and Opella, S. J. (1987) Dynamics of fd coat protein in bacteriophage, *Biochemistry 26*, 847−854.
51. Novabiochem (2004) Derivatives for phosphopeptide synthesis, in *Novabiochem 2004/2005 Catalog*, pp 192−194.
52. Simmerman, H. K. B., Lovelace, D. E., and Jones, L. R. (1989) Secondary Structure of Detergent-Solubilized Phospholamban, a Phosphorylatable, Oligomeric Protein of Cardiac Sarcoplasmic Reticulum, *Biochim. Biophys. Acta 997*, 322−329.
53. Buck, B., Zamoon, J., Kirby, T. L., DeSilva, T. M., Karim, C., Thomas, D., and Veglia, G. (2003) Overexpression, purification, and characterization of recombinant Ca-ATPase regulators for high-resolution solution and solid-state NMR studies, *Protein Expression Purif. 30*, 253−261.
54. Davis, J. H., Jeffrey, K. R., Bloom, M., and Valic, M. I. (1976) Quadrupolar echo deuteron magnetic resonance spectroscopy in ordered hydrocarbon chains, *Chem. Phys. Lett. 42*, 390−394.
55. Greenfield, M. S., Ronemus, A. D., Vold, R. L., Vold, R. R., Ellis, P. D., and Rady, T. E. (1987) Deuterium quadrupole-echo NMR spectroscopy III. Practical ascpects of line shape calculations for multiaxis rotational processes, *J. Magn. Reson. 72*, 89−107.
56. Seelig, G. R. (1977) Deuterium magnetic resonance: Theory and applications to lipid membranes, *Q. Rev. Biophys. 10*, 353−418.
57. Davis, J. H. (1983) The describtion of the membrane conformation, order and dynamics by ^{2}H-NMR, *Biochim. Biophys. Acta 737*, 117−171.
58. Keniry, M. A. (1989) Solid-state deutrerium nuclear magnetic resonance spectroscopy of proteins, *Methods Enzymol. 176*, 376−386.

59. Lee, K. C., and Cross, T. A. (1994) Side-Chain Structure and Dynamics at the Lipid-Protein Interface: Val of the Gramicidin A Channel, *Biophys. J. 66*, 1380−1387.
60. Massiot, D., Fayon, F., Capron, M., King, I., Le calve, S., Alonso, B., Durand, J. O., Bujoli, B., Gan, Z., and Hoatson, G. (2002) Modelling one- and two-dimensional solid-state NMR spectra, *Magn. Reson. Chem. 40*, 70−76.
61. http://www.avantilipids.com/TechnicalInformation.html (accessed May 14, 2006).
62. Wildman, K. A. H., Lee, D. K., and Ramamoorthy, A. (2003) Mechanism of lipid bilayer disruption by the human antimicrobial peptide, LL-37, *Biochemistry 42*, 6545−6558.
63. Ouellet, M., Voyer, N., and Auger, M. (2004) Conformational studies of artificial ion channel in interaction with model membranes by ^{2}H, ^{31}P and ^{15}N solid-state NMR spectroscopy. *Biophys. J. 86* (Part 2, Suppl. S), 204A−204A.
64. Whiles, J. A., Brasseur, R., Glover, K. J., Melacini, G., Komives, E. A., and Vold, R. R. (2001) Orientation and effects of mastoparan X on phospholipid bicelles, *Biophys. J. 80*, 280−293.
65. Smith, S. O., Kawakami, T., Liu, W., Ziliox, M., and Aimoto, S. (2001) Helical structure of phospholamban in membrane bilayers, *J. Mol. Biol. 313*, 1139−1148.
66. Lee, K. C., Hu, W., and Cross, T. A. (1993) ^{2}H NMR determination of the global correlation time of the gramicidin channel in a lipid bilayer, *Biophys. J. 65*, 1162−1167.
67. Mascioni, A., Karim, C., Zamoon, J., Thomas, D. D., and Veglia, G. (2002) Solid-state NMR and rigid body molecular dynamics to determine domain orientations of monomeric phospholamban, *J. Am. Chem. Soc. 124*, 9392−9393.
68. Hong, M., and Doherty, T. (2006) Orientation determination of membrane-disruptive proteins using powder samples and rotational diffusion: A simple solid-state NMR approach. *Chem. Phys. Lett. 432*, 296−300.

BI700749Q